Substitutional carbon doping of free-standing and Ru-supported BN sheets: A first-principles study

Originally published:

September 2017

Journal of Physics: Condensed Matter 29(2017), 415301

DOI: https://doi.org/10.1088/1361-648X/aa807c

Substitutional carbon doping of free-standing and Ru-supported BN sheets: A first-principles study

N. Berseneva[1], H.-P. Komsa[1], V. Vierimaa[1], T. Björkman[2,1], Z. Fan[1], A. Harju[1], M. Todorović[1], A. V. Krasheninnikov[1,3], and R. M. Nieminen[1]
[1]*Department of Applied Physics, Aalto University, P.O. Box 14100, 00076 Helsinki, Finland*
[2]*Physics/Department of Natural Sciences, Åbo Akademi, FI-20500 Turku, Finland and*
[3]*Helmholtz-Zentrum Dresden-Rossendorf, Institute of Ion Beam Physics and Materials Research, 01328 Dresden, Germany*
(Dated: April 9, 2017)

Development of spatially homogeneous mixed structures with boron (B), nitrogen (N) and carbon (C) atoms arranged in a honeycomb lattice is highly desirable, as they open a possibility to create stable two-dimensional materials with tunable band gaps. However, at least in the free-standing form, the mixed BCN system is energetically driven towards phase segregation to graphene and hexagonal BN. It is possible to overcome the segregation when BCN material is grown on a particular metal substrate, for example Ru(0001), but the stabilization mechanism is still unknown. With the use of density-functional theory we study the energetics of BN/Ru slabs, with different types of configurations of C substitutional defects introduced to the h-BN overlayer. The results are compared to the energetics of free-standing BCN materials. We found that the substrate facilitates the C substitution process in the h-BN overlayer. Thus, more homogeneous BCN material can be grown, overcoming the segregation into graphene and h-BN. In addition, we investigate the electronic and transport gaps in free-standing BCN structures, and assess their mechanical properties and stability. The band gap in mixed BCN free-standing material depends on the concentration of the constituent elements and ranges from zero in pristine graphene to nearly 5 eV in free-standing h-BN. This makes BCN attractive for application in modern electronics.

I. INTRODUCTION

Graphene[1] and hexagonal boron-nitride[2] (h-BN) sheets are two-dimensional (2D) materials that are just one atom thick. They both have honeycomb crystal structure with a small difference (about 2%) in lattice constants. Notably, while graphene is a semimetal, h-BN is a wide band gap insulator.

The similarities in the crystal structures and drastically different electronic properties point to the possibility of creating a mixed BCN material with a tunable band gap, which should depend on relative concentrations of B, C, and N atoms. Numerous calculations[3–18] have shown that the band gap in the mixed BCN system continuously varies from zero in pristine graphene to about 5 eV in h-BN.

The practical implementation of this idea has been difficult due to segregation of graphene and h-BN, as also predicted by simulations[19]. The samples grown by the chemical vapor deposition (CVD)[5,20] or pyrolysis[21] techniques consisted primarily of small patches of graphene and h-BN randomly distributed in the sample. The direct comparison of the measured and calculated electronic properties was not straightforward, as the calculations were done for periodic and well-ordered free-standing BCN systems, composed of domains or stripes of two materials[3,5–8].

Doping of BN nanostructures with carbon using in-situ electron-beam irradiation was demonstrated to yield BCN materials[22,23]. One more way to manufacture mixed BCN structure was shown to be low-energy ion beam irradiation[24] of free-standing graphene sheets. Commonly, chemical post-synthesis substitution of C atoms in graphene with B and N atoms (or other way around) is utilized when monolayer is supported by a substrate[8,25,26]. The Ru(0001) surface was experimentally shown to be a suitable for growing of BN-graphene heterostructures[27]. Moreover, Ru supports the growth of non-ordered BCN intermixing areas with no patterns[28], overcoming the phase segregation problem. By using Ru as a supporting material it is possible to avoid dealing with composite substrates (consisting of several materials[25]). This gives grounds to investigate the properties of non-ordered BCN intermixed materials and compare them to the properties of earlier investigated structures with BN and graphene islands.

Generally, very little is known about the energetics of BCN/Ru slab system and interaction between BCN overlayer and Ru (0001) substrate. This knowledge is crucially important for understanding the mechanism of forming BCN mixed systems. Moreover, there are still open questions regarding the electronic structure of the non-ordered BCN free-standing sheets and the correspondence between the fundamental semiconductor gap and transport gap. Carbon atoms incorporated in h-BN give rise to impurity states in the band gap, which may or may not affect the transport properties of the system. Since the estimation of the transport gap is done based on the conductivity of the material, the transport gap and electronic band gap may differ. Evaluating the transport gap value is important for the possible applications of the material.

In this paper we first study the energetics of different incorporated C substitutional defects into a free-standing h-BN sheet. Then we evaluate the effects of Ru(0001) substrate on the energetics of C substitution in a h-BN

overlayer. Finally, we investigate the electronic, transport and mechanical properties of free-standing BCN structures with different BN and C concentration ratios.

II. COMPUTATIONAL DETAILS

A. DFT calculations

We performed first-principles electronic structure calculations within the framework of the density functional theory (DFT) as implemented in the Vienna Ab initio Simulation Package (VASP)[29,30]. The one-electron Kohn-Sham wave functions were represented by a plane waves with a kinetic energy cutoff of 400 eV for slab calculations (where BN or BCN monolayer was placed on top of a Ru substrate) and 520 eV for free-standing systems. Gaussian smearing with a smearing width of 0.05 eV was used for geometry relaxation and band structure calculations of free-standing systems, while 0.1 eV was used for slab configurations. Structural optimizations of all atomic geometries were performed. To obtain optimal structures in the presence of weak van der Waals forces, a tight force convergence criteria of 0.002 eV/Å was adopted.

In order to prevent spurious interlayer interaction within the periodic supercell, a 20 Å vacuum spacing was introduced between adjacent h-BN layers (in the direction perpendicular to the sheet). In our slab calculations, the substrate consists of 3 layers of Ru (0001) with the lower layer fixed only in the z-direction allowing the system to adjust to the incorporated strain. The lattice constants of Ru and BN do not match. In order to construct a slab system with the minimum internal strain, we used a $12 \times 12 \times 3$ unit cell of Ru (lattice constant is 2.721 Å) and a $13 \times 13 \times 1$ unit cell of BN (lattice constant is 2.512 Å). The final BN/Ru or BCN/Ru slab supercells consist of 770 atoms.

Van der Waals interactions were taken into account in the slab calculations, using the AM05-VV10sol functional[31], which previously was shown to reproduce a Moiré pattern of h-BN overlayer close to the experimental one[32]. For free standing 2D systems, the exchange-correlation energy of the interacting electrons was described using the Perdew-Burke-Ernzerhof[33] (PBE) generalized gradient approximation, following previous works[16,34].

In the total-energy calculations, **k**-points in the Brillouin zone (BZ) were generated by the Monkhorst-Pack scheme with a Γ-centered grid. Specially, we used a $4 \times 4 \times 1$ mesh for $8 \times 8 \times 1$ and $10 \times 10 \times 1$ supercells of BN and BCN. In the case of graphene with BN substitutions, a $4 \times 4 \times 1$ mesh was used for $8 \times 8 \times 1$ supercells. For the slab systems, a $1 \times 1 \times 1$ **k**-point mesh was adopted.

B. Tight-binding calculations

In order to assess the system size effects in our simulations, DFT based calculations were complemented with the tight-binding (TB) modelling. The TB calculations were performed for BN and BCN sheets consisting of 1 million atoms (125×256 nm). We only considered the nearest-neighbour hopping t_0 with the strength of -2.7 eV between all atoms. Boron and nitrogen atoms were restricted to their own sublatices and modelled as sites with onsite-potential of $\pm t_0$[35]. The density of states (DOS) and conductivity were calculated using our implementation[36] of the real-space Kubo-Greenwood method[37], which scales linearly with system size and enables large system simulations. The DOS within this method is given by

$$\rho(E) = \mathrm{Tr}\left[\frac{2}{\Omega}\delta(E-H)\right], \tag{1}$$

where Ω is the system volume and the factor of 2 results from spin degeneracy. To calculate the conductivity, we consider the mean square displacement $\Delta X^2(E,t)$,

$$\rho(E)\Delta X^2(E,t) = \mathrm{Tr}\left[\frac{2}{\Omega}\delta(E-H)(X(t)-X)^2\right], \tag{2}$$

where $X(t)$ is the position operator in the Heisenberg representation. The conductivity is the time derivative of $\rho(E)\Delta X^2(E,t)$ multiplied by the electron charge e squared:

$$\sigma(E,t) = e^2\rho(E)\frac{\partial}{2\partial t}\Delta X^2(E,t). \tag{3}$$

A Chebyshev expansion was used to evaluate the delta functions and time evolution in the equations. For the delta functions the expansion was terminated after 3000 terms and the time evolution was stopped when the magnitude of the expansion coefficients drops below 10^{-15}. The traces were calculated by the random phase approximation[38] over 10 vectors. Because the energy resolution is finite, the energy gaps were defined as the region where the DOS value falls under 10^{-3} $1/t_0/atom$. The transport gap was determined from the conductivity data obtained with Eq. (3) as the region where the conductivity is less than 0.1 e^2/h for a t=1 ps corresponding to a sample length of 1 μm.

III. RESULTS AND DISCUSSION

A. Models of free-standing and slab systems

To analyze the formation process of BCN material, we explored different configurations of C substitutional defects in free-standing h-BN and in slab systems. Three types of arrangements for C substitutions in B and N positions were investigated in the free-standing system:

single substitutions C_B and C_N (where single B or N atom is substituted with C atom), in-pair substitutions (where 2 bonded C atoms replace 1 BN pair) and non-pair substitutions (spatially separated B and N atoms are substituted with 2 C atoms) (Fig. 1). The in-pair substitution configuration was motivated by experimental observations of doped BN sheets in TEM images[39], by experiments where ethylene molecules were used to obtain the BCN stuctures[26] and by synthesis utilizing bis-BN cyclohexane[40],

When constructing the slab model, it is possible to arrange a h-BN sheet on top of a Ru substrate in different ways with respect to the Ru surface atoms. We considered two different configurations (I and II) for positioning a h-BN layer on top of the metal substrate, as shown in Fig. 1 (a) and (b). These two structures are sufficient to represent the overall behaviour of the system and to account for all three high symmetry positions of B and N atoms with respect to the Ru atoms: *top* (on top of first layer Ru atoms), *hcp* (on top of Ru atoms of the second layer), and *fcc* (on top of hollow positions in between the Ru atoms). We note that configuration II (Fig. 1) has lower total energy and should be the ground state configuration.

Due to the lattice mismatch and the interaction of the overlayer with the Ru substrate, the h-BN sheet forms a Moiré pattern (Fig. 1 (c)). Valley (lower) areas are formed where N atoms are located on top of first layer of Ru atoms (*N-top* configuration). At the same time the hill (upper) areas are formed where N atoms are located in non-top positions (*hcp* or *fcc*). This agrees well with computed configurations reported earlier[41,42]. Also the size and shape of the hill and valley regions in our calculated Moiré pattern (Fig. 1 (c)) are in good agreement with the experimental STM images[28,43]. This confirms that the orientation of the BN sheet with respect to the Ru substrate is correct in our model.

To investigate the role of the substrate in the defect formation process, we constructed various substitutional defect configurations in the overlayer, including single C substitutions in B and N sites in either one of the high symmetry positions, C-pair substitutions, and selected non-pair C substitutional defects. The schematic representation of all C sites covered in this manuscript are marked by triangles in Fig. 1 (a) and (b).

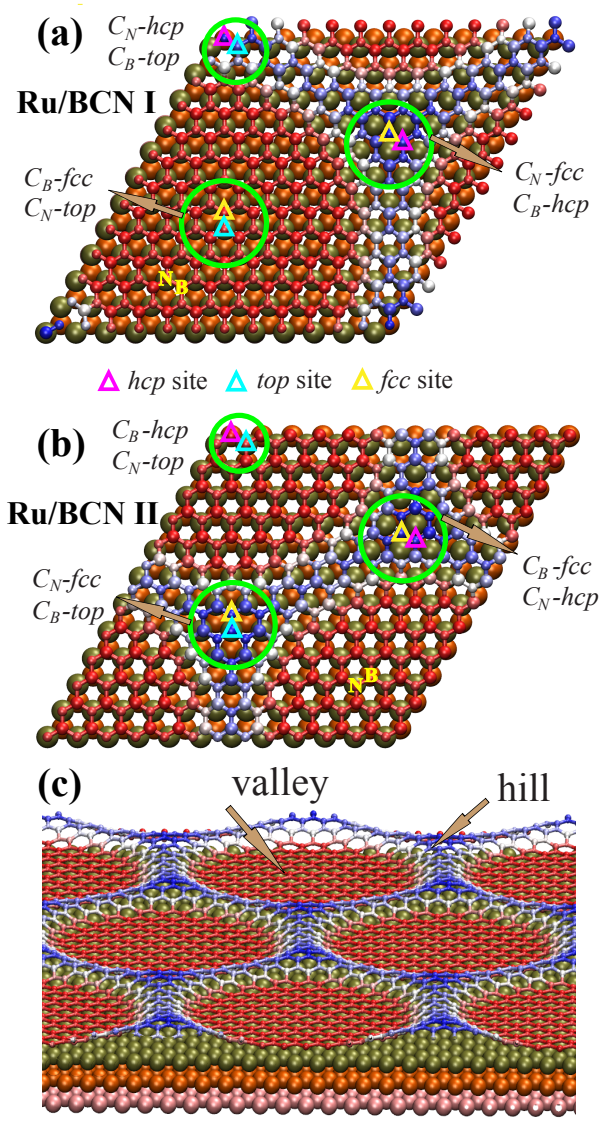

FIG. 1: (Color online) The Ru/BN slab supercells used in calculations. a) Configuration Ru/BCN I (N atom is located on top of Ru atom of the first layer), b) configuration Ru/BCN II (B atom is located on top of Ru atom of the first layer). Small triangles indicate the high symmetry positions of B and N atoms that we further substitute with C in different combinations. Their notations are specified in the text. B (bigger) and N (smaller) atoms of overlayer are colored by the elevation (blue color indicates valley and red color stands for hill regions). c) Periodically extended Ru/BN unit cell illustrating the development of the Moiré pattern in h-BN sheet located on top of Ru substrate. Green, orange, and pink atoms correspond to first, second, and third layer Ru atoms, respectively.

B. Energetics of C-substitutions

1. *Formation energy in free-standing BCN*

To understand which defect configurations are dominant, we studied the energetics of the systems by evaluating defect formation energy, E_f. For a free-standing layer, it is calculated as

$$E_f = E_{\rm tot}(BCN) - E_{\rm tot}(BN) + n_B\mu_B + n_N\mu_N - n_C\mu_C \quad (4)$$

where $E_{\rm tot}(BN)$ and $E_{\rm tot}(BCN)$ are total energies of a pure h-BN the system and a system with substitutional carbon defects, respectively. n_B and n_N are numbers of B and N atoms replaced by n_C carbon atoms.

The chemical potentials are chosen as in our previous works[16,34]. μ_C is equal to the chemical potential of a C

TABLE I: Defect formation energies E_f of different C substitutional defects and comparison between E_f for supported and free-standing BCN systems (ΔE_f).

		E_f, eV			ΔE_f, eV	
	Defect name	**Ru/BCN I**	**Ru/BCN II**	**free-standing**	**Ru/BCN I**	**Ru/BCN II**
1.	C_B-***top***	0.45	0.49	1.62	-1.40	-1.36
2.	C_B-***hcp***	0.69	2.09	1.62	-1.16	0.24
3.	C_B-***fcc***	1.92	0.54	1.62	0.07	-1.31
4.	C_N-***top***	1.09	1.12	4.23	-3.39	-3.36
5.	C_N-***hcp***	3.61	3.65	4.23	-0.88	-0.83
6.	C_N-***fcc***	2.24	3.67	4.23	-2.24	-0.81
7.	C_B-***fcc***C_N-***top(I)***/ C_B-***hcp***C_N-***top(II)***	1.95	1.91	1.96	-0.01	-0.05
8.	C_B-***top***C_N-***hcp(I)***/ C_B-***fcc***C_N-***hcp(II)***	1.91	1.99	1.96	-0.05	-0.03
9.	C_B-***hcp***C_N-***fcc(I)***/ C_B-***top***C_N-***fcc(II)***	1.92	2.01	1.96	-0.04	0.05
10.	C_B-***hcp***C_N-***top(I)***/ C_B-***top***C_N-***hcp(II)***	1.79	4.15	4.72	-2.93	-0.57
11.	C_B-***fcc***C_N-***fcc***	4.91	4.20	4.72	0.2	-0.52

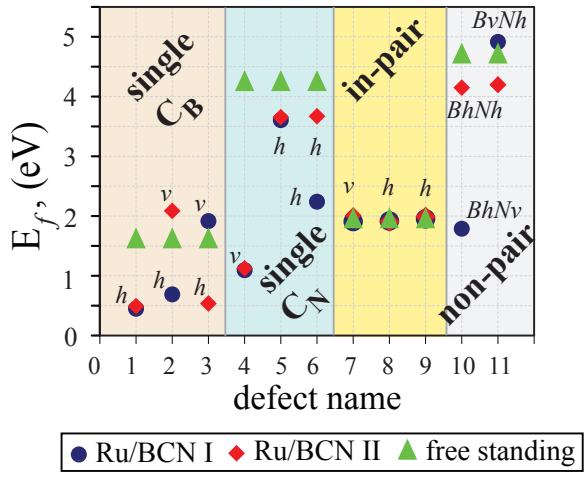

FIG. 2: (Color online) (a) Defect formation energies (E_f) for various types of C substitutional defects in Ru/BN slab and free-standing h-BN systems. Hill and valley defect locations in Moiré pattern are pointed out. Defect configurations are marked at the x-axis by numbers and explanation is given in Table I.

atom in graphene. We assume an N-rich environment, in which case the chemical potential of N is taken from the gas phase: μ_N=$E_{\rm tot}(N_2)/2$. B and N potentials are coupled by the equilibrium condition

$$\mu_{BN} = \mu_B + \mu_N \tag{5}$$

where μ_{BN} is the total energy per BN pair in the h-BN sheet. μ_B is obtained from Eq. (5).

Our calculations showed that in the case of single substitution, the formation energy strongly depends on the species of the substituted atom. With the above choice of chemical potentials and in a free-standing system, the formation of a neutral single C_B defect (a C atom in the position of a B atom) costs 1.62 eV, which is much less than the energy required for creation of C_N (4.23 eV). Nevertheless, the defect formation energy in the case of a double substitution is much smaller if a carbon pair is created (0.98 eV/C atom), as compared to the case where two C atoms are separated (2.36 eV/C atom). It is evident that in a free-standing h-BN matrix, in-pair C substitution is energetically favourable.

2. *Formation energy in supported BCN*

To explore the effect of the substrate on the energetics of substitutional impurities, defect formation energies in slab systems were calculated, using a formula similar to Eq. (4)

$$E_f = E_{\rm tot}(BCN/Ru) - E_{\rm tot}(BN/Ru) + n_B\mu_B + n_N\mu_N - n_C\mu_C \tag{6}$$

where $E_{\rm tot}(BN/Ru)$ and $E_{\rm tot}(BCN/Ru)$ are now the total energies of the pure BN/Ru system and a system with a C substitutional defect, respectively.

In contrast to the free-standing case, in supported systems the formation energy depends strongly not only on the substituted atom species, but also on the location of the defect in relation to the substrate atoms and the position in the Moiré pattern. Formation energies of different C substitutional defects and comparisons between E_f values for supported and free-standing BCN systems are collected in Table I and illustrated in Fig. 2.

As seen in the Table I, the formation of a single C_B defect in the overlayer costs less energy than the creation of a C_N located at the same position with respect to the substrate atoms. E_f of pair substitutions is independent of the pair position within the Moiré pattern. In

addition, the defect formation energy for in-pair substitutions is generally lower than for two distantly separated C atom substitutions. The one exception is the configuration where one of the two separated atoms is C_N-*top*, here E_f becomes smaller than for in-pair substitution.

To corroborate obtained results in a more complex system, we also performed calculations for the slab Ru/BCN system, where BCN overlayer contains 25% of C substitutional impurities in either in-pair or random configurations. The total energy of the slab system with in-pair C substitutions is smaller by approximately 0.045 eV/atom than with random substitutions.

In regard to single defects, for most C substitutions the formation energy in the slab system is lowered with respect to the same defect in a free-standing h-BN sheet. This suggests that the substitution process is easier in a supported system. There are a few exceptions though. The formation energies for C_B in *hcp* and *fcc* positions (located in valley region) are higher than in the free-standing h-BN sheet. E_f drops particularly strongly for C_N-*top* configuration in overlayer (almost to the level of E_f of C_B), suggesting that creation of this type of substitution is strongly favored. Single defect energetics is completely different for the free-standing system, where the formation energy of the C_N defect is much higher than C_B, making it difficult to create. In general, formation of isolated C_B is favored in the hill region, whereas C_N is favored in the valley region.

For double substitution, we observed that when two C atoms are separated within the h-BN sheet in slab system, their defect formation energies can be estimated from the sum of defect formation energies of respective isolated defects. This is different from the free-standing h-BN sheet, where the sum of E_f for isolated C_B and C_N defects is higher than E_f for two separated C substitutions located in the same system. In case of in-pair substitution the defect formation energies in free-standing h-BN and in BN/Ru slab are comparable. It arises from the strong interaction between C atoms arranged in pairs.

Summarising our results for supported systems, formation energies of single substitutional defects for BN/Ru slab systems are lower than the corresponding ones in the free-standing h-BN sheet (with only exceptions for configurations being single C_B atoms located in the valley regions). A system with random in-pair C substitutions is more energetically favourable than a system with random non-pair substitution. In addition, in Ref. 26, the process to form BCN overlayer was carried out using C_2H_4. It is a suitable way to make a compound with in-pair C-substitutions (since ethylene molecule contains a carbon pair already). Therefore, we mostly focus on the in-pair substitutions in our study of properties of free-standing BCN alloys.

3. Binding energy and Bader analysis for BCN/Ru systems

We also considered the changes in binding energy of BCN sheet to the Ru substrate depending on the position and configuration of substitutions. The binding energy was evaluated using the formula below.

$$E_{bind} = E_{tot}(BCN/Ru) - (E_{tot}(Ru) + E_{tot}(BCN)), \quad (7)$$

where $E_{tot}(BCN/Ru)$ is the total energy of the slab system (Ru substrate with a BCN or BN overlayer). $E_{tot}(Ru)$ and $E_{tot}(BCN)$ are the total energies of an isolated Ru substrate and a BCN/BN overlayer, respectively.

Comparison of Eq. (7) with Eq. (4) and Eq. (6) reveals that the changes in binding energy upon C substitution follow the changes in formation energy between the supported and the free-standing systems.

In most BCN configurations, the interaction between the substrate and overlayer becomes stronger than in case of a pure h-BN overlayer. The only exceptions causing weaker interactions are the structures which include C_B atoms (single or part of a non-pair configuration) located in the valley region. However, since these are the high formation energy configurations, we conclude that C substitution generally results in an increased binding energy between the overlayer and the substrate.

In addition, Bader charge analysis[44,45] was performed in slab systems for all considered carbon substitution configurations presented in Fig. 1 and Fig. 2. The results for BCN/Ru systems were compared to those for pure BN/Ru systems. On the whole, the BN and BCN sheets become negatively charged when placed on top of Ru substrate.

C_N substitutional atoms introduced in a BN overlayer gain nearly the same amount of charge (from 2.1 to 2.3 e) as N atoms in a pure BN overlayer (2.1 e). At the same time, there is almost no change in the local charge distribution in the adjacent B atoms. Such a situation persists independently of the C_N position with respect to Ru atoms and independently of the defect configurations (single, in-pair or distantly separated atoms).

C_B substitution introduces more changes to the BCN/Ru system than C_N. B atoms in pure h-BN overlayer loses 2.1 e. C_B loses less charge than B atoms in h-BN overlayer independently of the defect configuration and position with respect to Ru atoms. The value of C_B charge varies depending on the defect configuration. C_B as an isolated single defect or part of non-pair type substitution has a charge varying between +1.0 and +1.7 e. As a part of an in-pair substitution, the charge associated with C_B varies from +0.5 to +0.8 e. Accordingly, N and C_N atoms adjacent to C_B accept a smaller charge than N atom in pure h-BN overlayer.

C. Electronic and transport properties of free standing BCN sheet

The Ru substrate is needed only to support the production of a homogeneous BCN structure. After the overlayer is produced, it can be removed from the supporting metal. Since technological applications normally require BCN sheets exfoliated from the substrate, we concentrated further research on their characteristics.

Since h-BN is a wide band gap insulator and graphene is a semi-metal, there is a possibility to vary the band gap in the BCN system depending on the B, N, and C atom concentrations. We investigated the dependence of the band gap of BCN structures with random pair substitutions on the C concentration with DFT calculations, going beyond previously studied ordered structures. In order to account for system size effects, our research was complemented by TB calculations.

Following the common practice, special quasi-random structures (SQS)[46,47] are used to construct models, which efficiently mimic random substitutional alloys. In order to model random pair substitution with DFT calculations, a two-step scheme was adopted. We first constructed a SQS for C substitution in the B sub-lattice of h-BN using the ATAT software[48]. In the second step, for each C_B site we chose randomly one of the three neighbouring N sites and substituted it with another C atom to form a pair. If all three neighbouring N sites were already filled, the second C atom was placed at any free N sub-lattice site. This approach should guarantee random in-pair substitution even if the orientation of pairs does not follow the SQS procedure. To obtain the dependence of the DFT electronic band gap on C concentration in BCN system, we performed averaging over several configurations with the same starting SQS structure, but different pair orientations. In the case of alloys with carbon concentration higher than 50%, the substitution process was organized the same way as discribed above but with graphene as a starting system. We first constructed a SQS for B substitution in either one of the graphene C sub-lattices and then substituted randomly one of the C neighbours by N atom.

The method to generate the atomic models for TB simulations is mostly the same as for DFT calculation. The site for the first atom of the substitutional pair is chosen randomly from the system. If all three neighbours of this site have already been substituted, a new site is randomized until an eligible one is found. The system with higher concentration is always constructed taken the system with smaller concentration as a starting point for substitution process.

At first, we considered the electronic structure of single impurities. In the case of C_B, there is one impurity level in the band gap, located in the upper part or the gap. Similarly, in the case of C_N, there is one impurity level in the lower part of the gap. The impurity levels are occupied by one electron in both cases. In the case of the C pair, the impurity levels move closer to the band edges due to the strong interaction between the two carbon atoms forming the pair. Moreover, the defect state close to valence band maximum (VBM) is occupied by two electrons and the one close to conduction band minimum (CBM) is unoccupied.

The same locations of impurity states were observed also in the electronic structures and DOS of BCN systems with higher C concentrations. However, the distribution of states becomes broader as the defect concentration increases due to interaction between defects. We illustrate the example of electronic structure of BCN alloys with 6.25% of C concentration (in-pair and non-pair substitution) by plotting their effective band structures[49] and DOS in Fig. 3. At higher carbon concentration, impurity states related to in-pair substitution appear within the gap near the band edges. In the case of random non-pair substitution, so many impurity levels appear that the gap disappears even at such moderate concentration.

Band gap dependence on the C-concentration in a BCN system obtained with DFT and TB approaches is shown in Fig. 4. The starting point is the band gap of pure h-BN and the final one is the zero gap of graphene. DOS band gaps obtained with TB show the same trend as a curve for electronic band gaps calculated with DFT. In both cases there is a drop in band gap value after incorporating the first portion of C substitutional impurities, which can be ascribed to the introduction of defect states inside the gap. The DFT curve deviates from the TB result at concentrations where the ratio of BN/C constituents in the system is close to 50% BN and 50% C. This difference is likely caused by finite size effects in the DFT model. As seen from Fig. 4, although relatively small systems were considered in the DFT calculations in comparison to TB, the trend for band gap dependence is the same in both cases.

We have also calculated with TB approach how the transport gap depends on the C-concentration. Fig. 4 shows that the transport gap is larger than the electronic band gap for all concentrations. This suggests that the states near the band edges are strongly localized and do not conduct. At small carbon substitution concentrations, the transport gap is larger than the transport gap for pure BN. This is because the impurity states at carbon atoms need to be orthogonal to the BN states, pushing them away from the Fermi energy.

We conclude that it is possible to make a free-standing BCN structure with a variable band gap, depending on B, N, and C atom concentration in the system.

D. Mechanical properties of BCN monolayer

Finally, with DFT we analyzed the mechanical properties of BCN systems and their stability at finite temperatures. Previous calculations have revealed stress-strain relations[50], and how the band gap[51], work function[52], piezoelectric constants[53] and optical properties[54] change under applied strain. However, these studies considered

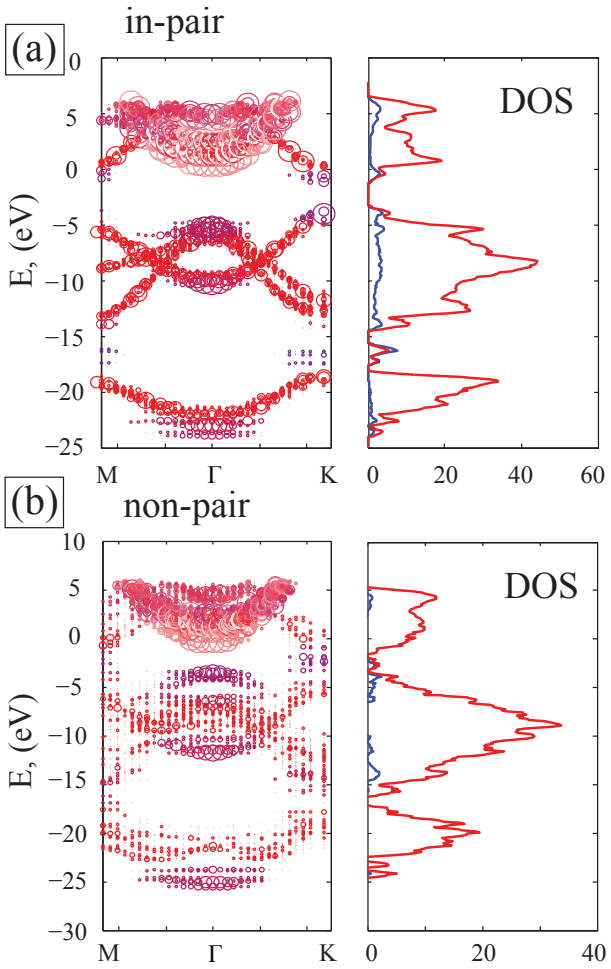

FIG. 3: (Color online) Effective band structure and DOS for free-standing h-BN system with 6.25% of C concentration in (a) in-pair and (b)non-pair C substitutions. B and N atoms are equally substituted. In the effective band structure, size of the circle represents the supercell wave function projection to a plane wave with wave vector k from the primitive cell Brillouin zone. The color represents the wave function projection to different atoms (B/N: red; C: blue). Red and blue curves in DOS plot represent the DOS for BN and carbon respectively.

various crystalline or highly ordered configurations of C, B, and N (including BN or C islands embedded into graphene or BN[55]); an investigation of mechanical properties and stability of the systems was not done for random configurations.

We explored a free-standing BCN system with 50% of C substitutional atoms as well as pure h-BN and graphene. We computed the stress-strain curves, where the tensile strain is applied in only X (zig-zag), only Y (arm-chair) directions, and simultaneously in X and Y directions (biaxial) (Fig. 5). The mixed system has the characteristics between graphene and h-BN at low strains, but it will become less durable at high strains, as the mixture shows more broken bonds within the structure.

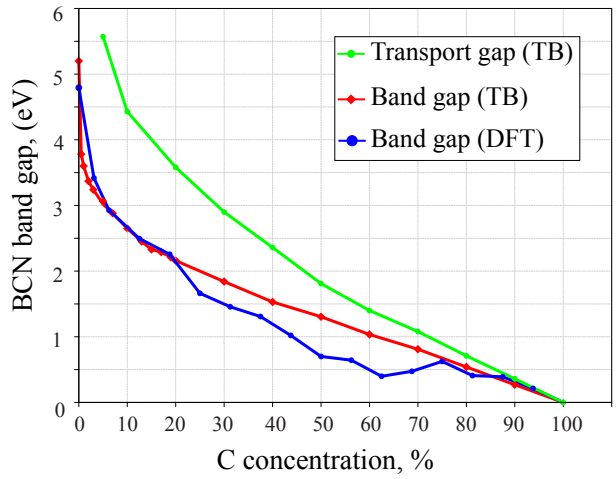

FIG. 4: (Color online) Dependence of band gap in BCN system as a function of C concentration. Blue curve displays DFT electronic band gap. Red curve represents DOS band gap obtained within the tight-binding approach. Green curve demonstrates the transport gap calculated within tight-binding approach.

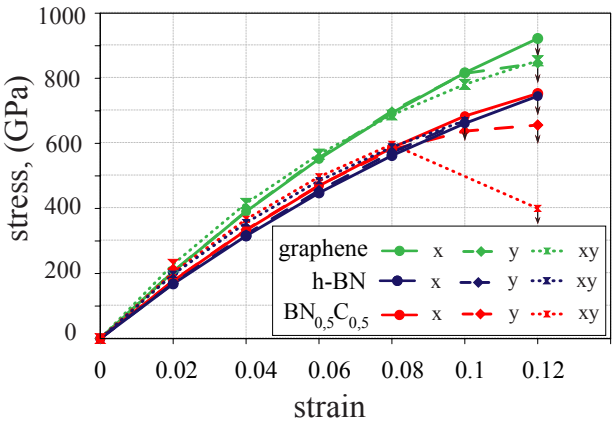

FIG. 5: (Color online) Strain-stress curves are shown for the pure graphene, pure h-BN and for BCN system with 50 % C and 50 % BN ($BN_{0.5}C_{0.5}$). Solid, dashed, and dotted curves represent system behaviour when the tensile strain is applied, accordingly, in only X (arm-chair) and only Y (zig-zag) directions, as well as simultaneously in X and Y directions (biaxial). The stress is measured in the same direction as an applied stain. Arrows indicate that breakage occurs in the structures.

This observation is in good agreement with experimental measurements reported in Ref. 56, which also conclude that graphene doped with BN is more sensitive to applied strain than the pure system, which makes it more suitable for strain sensor application.

IV. CONCLUSIONS

In conclusion, our results provide microscopic insight into the structures and properties of BCN systems supported by Ru. Our study showed that a homogeneous BCN structure should be easier to obtain when grown on top of a Ru substrate, inferred from the lowered formation energies of C substitutional defects in the BN lattice due to interaction with the substrate. Moreover, we demonstrated that the band gap in free-standing disordered BCN material with in-pair C-substitutions can be continuously varied depending on the concentration of the constituent elements. Conductivity calculations demonstrated that transport gaps are somewhat larger than the electronic fundamental gap for corresponding systems. Finally, the mechanical properties illustrated that BCN materials are robust, although more sensitive to applied strain than pure graphene and h-BN. Overall, our work indicates the possibility to create homogeneous BCN structures with desired electronic properties which could fulfill the needs of modern electronics in the semiconductors with tunable band gaps.

V. ACKNOWLEDGMENT

We thank the Academy of Finland for the support under Project No. 286279 and through its Centres of Excellence Programme (2012-2017) under Project No. 251748 and Suomalainen Tiedeakatemia (N. B., personal grant). We also thank the CSC-IT Center for Science Ltd and the Aalto Science-IT project for generous grants of computer time.

[1] A. K. Geim and K. S. Novoselov, Nature Mater. **6**, 183 (2007).
[2] D. Golberg, Y. Bando, Y. Huang, T. Terao, M. Mitome, C. Tang, and C. Zhi, ACS Nano **4**, 2979 (2010).
[3] Q. Peng and S. De, Physica E: Low-dimensional Systems and Nanostructures **44**, 1662 (2012), ISSN 1386-9477, URL http://www.sciencedirect.com/science/article/pii/S1386947712001579.
[4] J. Zhu, S. Bhandary, B. Sanyal, and H. Ottosson, The Journal of Physical Chemistry C **115**, 10264 (2011), http://dx.doi.org/10.1021/jp2016616, URL http://dx.doi.org/10.1021/jp2016616.
[5] B. Muchharla, A. Pathak, Z. Liu, L. Song, T. Jayasekera, S. Kar, R. Vajtai, L. Balicas, P. M. Ajayan, S. Talapatra, et al., Nano Letters **13**, 3476 (2013), pMID: 23859076, http://dx.doi.org/10.1021/nl400721y, URL http://dx.doi.org/10.1021/nl400721y.
[6] K.-T. Lam, Y. Lu, Y. P. Feng, and G. Liang, Applied Physics Letters **98**, 022101 (2011), URL http://scitation.aip.org/content/aip/journal/apl/98/2/10.1063/1.3535604.
[7] P. Lu, Z. Zhang, and W. Guo, The Journal of Physical Chemistry C **115**, 3572 (2011), http://dx.doi.org/10.1021/jp110217t, URL http://dx.doi.org/10.1021/jp110217t.
[8] Y. Gong, G. Shi, Z. Zhang, W. Zhou, J. Jung, W. Gao, L. Ma, Y. Yang, S. Yang, G. You, et al., Nat Commun **5** (2014), URL http://dx.doi.org/10.1038/ncomms4193.
[9] G. Seol and J. Guo, Applied Physics Letters **98**, 143107 (2011), URL http://scitation.aip.org/content/aip/journal/apl/98/14/10.1063/1.3571282.
[10] Z. Huang, V. H. Crespi, and J. R. Chelikowsky, Phys. Rev. B **88**, 235425 (2013), URL http://link.aps.org/doi/10.1103/PhysRevB.88.235425.
[11] L. Song, L. Balicas, D. J. Mowbray, R. B. Capaz, K. Storr, L. Ci, D. Jariwala, S. Kurth, S. G. Louie, A. Rubio, et al., Phys. Rev. B **86**, 075429 (2012), URL http://link.aps.org/doi/10.1103/PhysRevB.86.075429.
[12] A. Ramasubramaniam and D. Naveh, Phys. Rev. B **84**, 075405 (2011), URL http://link.aps.org/doi/10.1103/PhysRevB.84.075405.
[13] S. Jungthawan, S. Limpijumnong, and J.-L. Kuo, Phys. Rev. B **84**, 235424 (2011), URL http://link.aps.org/doi/10.1103/PhysRevB.84.235424.
[14] J. d. R. Martins and H. Chacham, Phys. Rev. B **86**, 075421 (2012), URL http://link.aps.org/doi/10.1103/PhysRevB.86.075421.
[15] S. Cahangirov and S. Ciraci, Phys. Rev. B **83**, 165448 (2011), URL http://link.aps.org/doi/10.1103/PhysRevB.83.165448.
[16] N. Berseneva, A. Gulans, A. V. Krasheninnikov, and R. M. Nieminen, Phys. Rev. B **87**, 035404 (2013), URL http://link.aps.org/doi/10.1103/PhysRevB.87.035404.
[17] J. da Rocha Martins and H. Chacham, ACS Nano **5**, 385 (2011), pMID: 21186786, http://dx.doi.org/10.1021/nn101809j, URL http://dx.doi.org/10.1021/nn101809j.
[18] D. Kaplan, G. Recine, and V. Swaminathan, Applied Physics Letters **104**, 133108 (2014), URL http://scitation.aip.org/content/aip/journal/apl/104/13/10.1063/1.4870769.
[19] K. Yuge, Phys. Rev. B **79**, 144109 (2009), URL http://link.aps.org/doi/10.1103/PhysRevB.79.144109.
[20] L. Ci, L. Song, C. H. Jin, D. Jariwala, D. X. Wu, Y. J. Li, A. Srivastava, Z. F. Wang, K. Storr, L. Balicas, et al., Nature Mater. **9**, 430 (2010).
[21] C. Huang, C. Chen, M. Zhang, L. Lin, X. Ye, S. Lin, M. Antonietti, and X. Wang, Nat Commun **6** (2015), URL http://dx.doi.org/10.1038/ncomms8698.
[22] X. Wei, M.-S. Wang, Y. Bando, and D. Golberg, ACS Nano **5**, 2916 (2011), pMID: 21425863, http://dx.doi.org/10.1021/nn103548r, URL http://dx.doi.org/10.1021/nn103548r.
[23] X. Wei, M.-S. Wang, Y. Bando, and D. Golberg, Journal of the American Chemical Society **132**, 13592 (2010), pMID: 20836492, http://dx.doi.org/10.1021/ja106134s, URL http://dx.doi.org/10.1021/ja106134s.
[24] D. Kepaptsoglou, T. P. Hardcastle, C. R. Seabourne, U. Bangert, R. Zan, J. A. Amani, H. Hofsäss, R. J. Nicholls, R. M. D. Brydson, A. J. Scott, et al., ACS Nano

9, 11398 (2015).

[25] G. Kim, H. Lim, K. Y. Ma, A.-R. Jang, G. H. Ryu, M. Jung, H.-J. Shin, Z. Lee, and H. S. Shin, Nano Letters **15**, 4769 (2015), pMID: 26083832, http://dx.doi.org/10.1021/acs.nanolett.5b01704, URL http://dx.doi.org/10.1021/acs.nanolett.5b01704.

[26] J. Lu, K. Zhang, X. F. Liu, H. Zhang, T. C. Sum, A. H. C. Neto, and K. P. Loh, Nat Commun **4**, 2681 (2013), URL http://dx.doi.org/10.1038/ncomms3681.

[27] P. Sutter, Y. Huang, and E. Sutter, Nano Letters **14**, 4846 (2014), pMID: 25054434, http://dx.doi.org/10.1021/nl502110q, URL http://dx.doi.org/10.1021/nl502110q.

[28] P. Sutter, R. Cortes, J. Lahiri, and E. Sutter, Nano Letters **12**, 4869 (2012), pMID: 22871166, http://dx.doi.org/10.1021/nl302398m, URL http://dx.doi.org/10.1021/nl302398m.

[29] G. Kresse and J. Furthmüller, Comp. Mat. Sci. **6**, 15 (1996).

[30] G. Kresse and J. Furthmüller, Phys. Rev. B **54**, 11169 (1996).

[31] T. Björkman, Phys. Rev. B **86**, 165109 (2012).

[32] A. V. Krasheninnikov, N. Berseneva, D. G. Kvashnin, J. Enkovaara, T. Björkman, P. B. Sorokin, D. V. Shtansky, R. Nieminen, and D. Golberg, Journal of Physical Chemistry C **118**, 26894 (2014).

[33] J. P. Perdew, K. Burke, and M. Ernzerhof, Phys. Rev. Lett. **77**, 3865 (1996).

[34] N. Berseneva, A. V. Krasheninnikov, and R. M. Nieminen, Phys. Rev. Lett. **107**, 035501 (2011), URL http://link.aps.org/doi/10.1103/PhysRevLett.107.035501.

[35] J. Jung, Z. Qiao, Q. Niu, and A. H. MacDonald, Nano Letters **12**, 2936 (2012).

[36] Z. Fan, A. Uppstu, T. Siro, and A. Harju, Computer Physics Communications **185**, 28 (2014).

[37] S. Roche and D. Mayou, Phys. Rev. Lett. **79**, 2518 (1997).

[38] A. Weiße, G. Wellein, A. Alvermann, and H. Fehske, Rev. Mod. Phys. **78**, 275 (2006), URL http://link.aps.org/doi/10.1103/RevModPhys.78.275.

[39] O. L. Krivanek, M. F. Chisholm, V. Nicolosi, T. J. Pennycook, G. J. Corbin, N. Dellby, M. F. Murfitt, C. S. Own, Z. S. Szilagyi, M. P. Oxley, et al., Nature **464**, 571 (2010).

[40] S. Beniwal, J. Hooper, D. P. Miller, P. S. Costa, G. Chen, S.-Y. Liu, P. A. Dowben, E. C. H. Sykes, E. Zurek, and A. Enders, ACS Nano **0**, null (0), pMID: 28165713, http://dx.doi.org/10.1021/acsnano.6b08136, URL http://dx.doi.org/10.1021/acsnano.6b08136.

[41] J. Gómez Díaz, Y. Ding, R. Koitz, A. P. Seitsonen, M. Iannuzzi, and J. Hutter, Theoretical Chemistry Accounts **132**, 1 (2013), ISSN 1432-2234, URL http://dx.doi.org/10.1007/s00214-013-1350-z.

[42] R. Laskowski, P. Blaha, and K. Schwarz, Phys. Rev. B **78**, 045409 (2008), URL http://link.aps.org/doi/10.1103/PhysRevB.78.045409.

[43] A. Goriachko, Y. He, M. Knapp, , H. Over, M. Corso, T. Brugger, S. Berner, J. Osterwalder, and T. Greber, Langmuir **23**, 2928 (2007), pMID: 17286422, http://dx.doi.org/10.1021/la062990t, URL http://dx.doi.org/10.1021/la062990t.

[44] R. F. W. Bader, New York: Oxford University Press (1990).

[45] W. Tang, E. Sanville, and G. Henkelman, Journal of Physics: Condensed Matter **21**, 084204 (2009), URL http://stacks.iop.org/0953-8984/21/i=8/a=084204.

[46] A. Zunger, S.-H. Wei, L. G. Ferreira, and J. E. Bernard, Phys. Rev. Lett. **65**, 353 (1990), URL http://link.aps.org/doi/10.1103/PhysRevLett.65.353.

[47] A. van de Walle, P. Tiwary, M. de Jong, D. Olmsted, M. Asta, A. Dick, D. Shin, Y. Wang, L.-Q. Chen, and Z.-K. Liu, Calphad **42**, 13 (2013), ISSN 0364-5916, URL http://www.sciencedirect.com/science/article/pii/S0364591613000540.

[48] A. Walle and G. Ceder, Journal of Phase Equilibria **23**, 348 (2002), ISSN 1054-9714, URL http://dx.doi.org/10.1361/105497102770331596.

[49] V. Popescu and A. Zunger, Phys. Rev. Lett. **104**, 236403 (2010), URL http://link.aps.org/doi/10.1103/PhysRevLett.104.236403.

[50] L. Jiao, M. Hu, Y. Peng, Y. Luo, C. Li, and Z. Chen, Journal of Solid State Chemistry **244**, 120 (2016), ISSN 0022-4596, URL http://www.sciencedirect.com/science/article/pii/S0022459616303589.

[51] R. Nascimento, J. da Rocha Martins, R. J. C. Batista, and H. Chacham, The Journal of Physical Chemistry C **119**, 5055 (2015), http://dx.doi.org/10.1021/jp5101347, URL http://dx.doi.org/10.1021/jp5101347.

[52] Y. Fujimoto and S. Saito, Phys. Rev. B **93**, 045402 (2016), URL http://link.aps.org/doi/10.1103/PhysRevB.93.045402.

[53] K. Shimada, T. Sota, K. Suzuki, and H. Okumura, Japanese Journal of Applied Physics **37**, L1421 (1998), URL http://stacks.iop.org/1347-4065/37/i=12A/a=L1421.

[54] J. H. Mokkath and U. Schwingenschlogl, J. Mater. Chem. C **2**, 8322 (2014), URL http://dx.doi.org/10.1039/C4TC01640H.

[55] S. Zhao and J. Xue, Journal of Physics D: Applied Physics **46**, 135303 (2013), URL http://stacks.iop.org/0022-3727/46/i=13/a=135303.

[56] S.-H. Pan, H. Medina, S.-B. Wang, L.-J. Chou, Z. M. Wang, K.-H. Chen, L.-C. Chen, and Y.-L. Chueh, Nanoscale **6**, 8635 (2014), URL http://dx.doi.org/10.1039/C4NR00495G.